New insights of the Sicily Channel and southern Tyrrhenian Sea variability

Milena Menna, Pierre-Marie Poulain, Daniele Ciani, Andrea M. Doglioli, Giulio Notarstefano, Riccardo Gerin, Marie-Hélène Rio, Rosalia Santoleri, Adam Gauci, Aldo Drago

AUTHOR = Menna, Milena and Poulain, Pierre-Marie and Ciani, Daniele and Doglioli, Andrea and Notarstefano, Giulio and Gerin, Riccardo and Rio, Marie-Helene and Santoleri, Rosalia and Gauci, Adam and Drago, Aldo

TITLE = New Insights of the Sicily Channel and Southern Tyrrhenian Sea Variability

JOURNAL = Water

VOLUME = 11

YEAR = 2019

NUMBER = 7

ARTICLE-NUMBER = 1355

DOI = 10.3390/w11071355

ISSN = 2073-4441

URL = https://www.mdpi.com/2073-4441/11/7/1355

ABSTRACT = The dynamics of the Sicily Channel and the southern Tyrrhenian Sea are highly influenced by the seasonal variability of the Mediterranean basin-wide circulation, by the interannual variability of the numerous mesoscale structures present in the Channel, and by the decadal variability of the adjacent Ionian Sea. In the present study, all these aspects are investigated using in-situ (Lagrangian drifter trajectories and Argo float profiles) and satellite data (Absolute Dynamic Topography, Sea Level Anomaly, Sea Surface Temperature, wind products) over the period from 1993 to 2018. The availability of long time series of data and high-resolution multi-sensor surface currents allow us to add new details on the circulation features and on their driving mechanisms and to detect new permanent eddies not yet described in literature. The structures prevailing in winter are mainly driven by wind, whereas those prevailing in summer are regulated by topographical forcing on surface currents. The strength of the surface structures located at the western entrance of the Ionian Sea and of the mesoscale activity along the northern Sicily coast is modulated by the large-scale internal variability. The vertical hydrological characteristics of these mesoscale eddies are delineated using the Argo float profiles inside these structures

water

MDPI

Article

New insights of the Sicily Channel and southern Tyrrhenian Sea variability

Milena Menna[1], Pierre-Marie Poulain[1,2], Daniele Ciani[3], Andrea Doglioli[4], Giulio Notarstefano[1], Riccardo Gerin[1], Marie-Helene Rio[5], Rosalia Santoleri[3], Adam Gauci[6], Aldo Drago[6]

[1] Istituto nazionale di Oceanografia e Geofisica Sperimentale, OGS, Sgonico (TS), Italy; mmenna@inogs.it, rgerin@inogs.it, gnotarstefano@inogs.it
[2] Centre for Marine Research and Experimentation, CMRE, La Spezia, Italy; Pierre-Marie.Poulain@cmre.nato.int
[3] Consiglio Nazionale delle Ricerche, Istituto di Scienze Marine, CNR-ISMAR, Via del Fosso del Cavaliere, 100, 00133, Rome, Italy; daniele.ciani@cnr.it, rosalia.santoleri@cnr.it
[4] Mediterranean Institute of Oceanography, MIO, Marseilles, France; andrea.doglioli@univ-amu.fr
[5] European Space Research Institute, ESA-ESRIN, Frascati, Italy; Marie-Helene.RIO@esa.int
[6] Physical Oceanography Research Group, Department of Geosciences, University of Malta, Malta; adam.gauci@um.edu.mt, aldo.drago@um.edu.mt

* Correspondence: mmenna@inogs.it; Tel.: +39 0402140302

Received: date; Accepted: date; Published: date

Abstract: The dynamics of the Sicily Channel and southern Tyrrhenian Sea is highly influenced by the seasonal variability of the Mediterranean basin-wide circulation, by the interannual variability of the numerous mesoscale structures present in the Channel, and by the decadal variability of the adjacent Ionian Sea. In the present study, all these aspects are investigated using in-situ (Lagrangian drifter trajectories and Argo float profiles) and satellite data (Absolute Dynamic Topography, Sea Level Anomaly, Sea Surface Temperature, wind products) over the period 1993-2018. The availability of long time series of data and high resolution multi-sensor surface currents, allow us to add new details on the circulation features and on their driving mechanisms and to detect new permanent eddies not yet described in literature. The structures prevailing in winter are mainly driven by wind, whereas those prevailing in summer are regulated by topographical forcing on surface currents. The strength of the surface structures located at the western entrance of the Ionian Sea and of the mesoscale activity along the northern Sicily coast is modulated by the large–scale internal variability. The vertical hydrological characteristics of these mesoscale eddies are delineated using the Argo float profiles inside these structures.

Keywords: Sicily Channel; spatial and temporal variability; mesoscale eddies

1. Introduction

Thanks to its location in the centre of the Mediterranean Basin, the Sicily Channel (SC) plays a crucial role in connecting the western and eastern Mediterranean basins and modulating their exchange of the surface and intermediate waters [1,2]. The SC is characterised by a complex bottom topography, with submarine ridge and shallow banks, and it is delimited to the north by the Tyrrhenian Sea and the Sicily coast, to the south by the Libyan coast, to the west by the Tunisia coast and to the east by the Ionian Sea (Figure 1a). Its circulation can be schematized on the vertical as a two-layer exchange with an eastward flow of Atlantic Water (AW) superposed to a westward flow of intermediate water, dominated by the Levantine Intermediate Water (LIW) [3]. Microstructure measurements taken in the SC show that it is a hotspot for turbulent mixing [4,5]. Consequently, the SC is a key area for the

regulation of salt exchanges between Eastern and Western basins, with an impact on the deep-water formation processes [6].

Circulation in the upper layer of the SC and in the southern Tyrrhenian Sea is mainly dictated by the large-scale Mediterranean thermohaline circulation, the wind-driven currents along the shelf, the upwelling events off Sicily, the sub-basin scale and mesoscale permanent and quasi-permanent structures [1,3,7,8,9]. The recent results of AW circulation schemes, derived by numerical model simulation [1,3], are summarized in Figure 1b (both permanent and seasonal circulation structures are depicted with the same colour in Figure 1b; more details on the time scales and variability of these structures are available in Section 3; acronyms are defined in Table1). The sub-basin scale structures are characterised by a prominent seasonal variability [9-12] associated with large wind stress fluctuations [13]. The numerous mesoscale structures located in the SC are mainly driven by the instability of the large scale circulation, by the the interactions between currents and bathymetry and by the direct wind forcing [1].

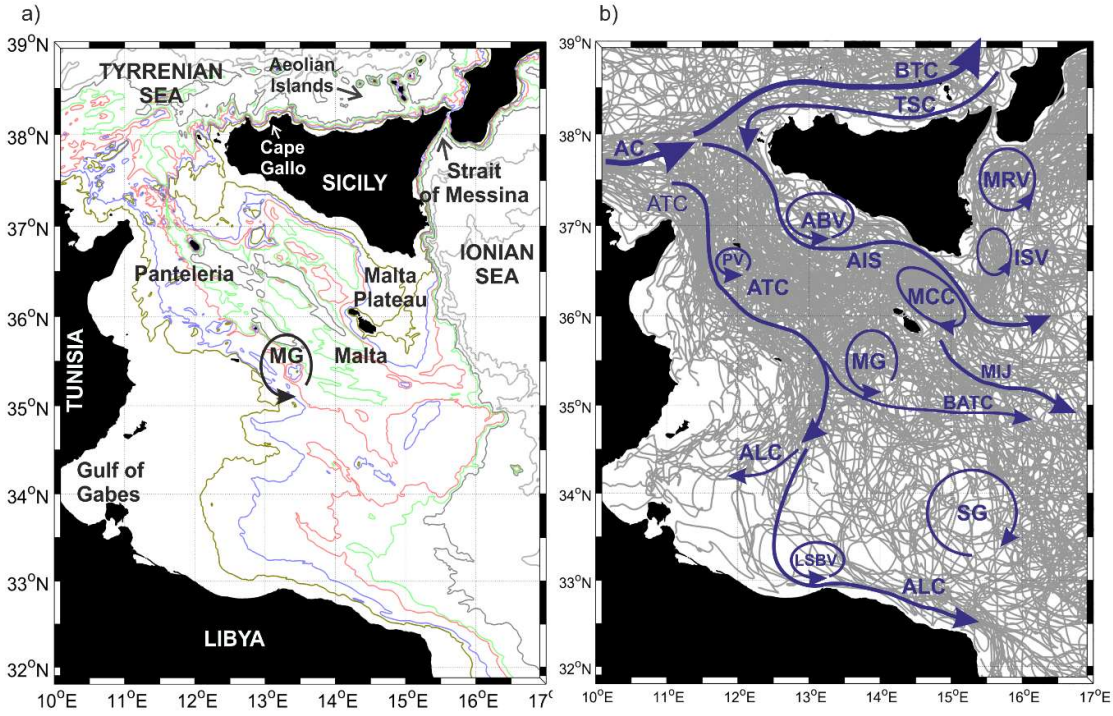

Figure 1. (a) Bathymetry of the SC (100 m, 200 m, 400 m, 600 m, 1000 m, 2000 m isobaths) and geographical references. (b) Low-pass filtered drifter trajectories in the SC between 1993 and 2018 superimposed with the schematic surface circulation adapted from [1] and [3]; acronyms are listed in Table 1.

Nowadays, the availability of long time series of in-situ and satellite data and of sophisticated statistical techniques, allow us to add new details on the mesoscale features and on their driving mechanisms. In this study, Lagrangian drifter trajectories, Argo float profiles and satellite data (Absolute Dynamic Topography, Sea Level Anomaly, Sea Surface Temperature, wind products) are used to describe the surface circulation of the SC and the southern Tyrrhenian Sea over the period 1993-2018. The simultaneous use of all these datasets leads to overcome the intrinsic limitations of each of them, e.g. the accurate but discontinuous spatial and temporal drifter sampling and the low accuracy of altimetry gridded data in the identification of the mesoscale field [14]. Moreover, the knowledge of the mesoscale field is ameliorated using the multi-sensor currents (defined hereafter as 'optimal currents') derived from the merging of the satellite altimetry data and the Sea Surface Temperature (SST) fields [15]. This product enables to improve the description of eddy dynamics and

non geostrophic dynamical features [15]. The vertical structures and the hydrological characteristics of the mesoscale eddies are delineated using the Argo float profiles inside these structures. All these data and products enhance the knowledge on the temporal variability of the mesoscale structures, with detection of new features not yet described in the literature, and the addition of new insights on the formation mechanisms of these structures.

2. Materials and Methods

The datasets used for this study are:

- The OGS Mediterranean drifter dataset in the SC and Southern Tyrrhenian Sea, composed of 377 drifter tracks collected between 1993 and 2018 (Figure 1b). Drifter data were retrieved from the OGS own projects, but also from databases collected by other research institutions and by international data centres (Global Drifter Program, SOCIB, CORIOLIS, MIO, etc.). These data were cleaned from potential outliers and elaborated with standard procedures (editing, manual editing and interpolation; [16,17]). In particular, we use the low-pass filtered and interpolated (6 hours) drifter tracks which represent the near-surface currents between 0 m and 15 m depth.

- The daily (1/8º Mercator projection grid) Absolute Dynamic Topography (ADT) and correspondent Absolute Geostrophic Velocities (AGV) derived from altimeter and distributed by CMEMS in the period 1993-2018 (product user manual CMEMS-SL-QUID_008-032-051). The ADT was obtained by the sum of the sea level anomaly and a 20-years synthetic mean estimated by [18] over the 1993-2012 period.

- The Argo float vertical profiles of temperature and salinity from the upper 2000 m of the water column and the horizontal currents displacements at the parking depth. In the Mediterranean Sea, the Argo floats are generally programmed to execute 5-day cycles with a drifting depth of 350 m (parking depth). Additionally, they alternate the profiling depth between 700 m and 2000 m (see the MedArgo program in [19]). When a float drifts in a shallow area and touches the ground, it can increase its buoyancy to get away from bottom, or can stay there until it is time to ascent (depending on how it is programmed). Information about grounding events is contained in the Argo float trajectory file. Among all the data available in the Mediterranean Sea, we selected of the part of the Argo floats trajectories which correspond to a float entrapped in the mesoscale structures of the SC and southern Tyrrhenian Sea. These data were used to define the vertical hydrographic peculiarities of the mesoscale features. Details about the missions of the seven floats selected for this work are listed in Table 2.

- The optimal currents, estimated by [15] and presently available in the period 2012-2016. This product was used to confirm the occurrence of the mesoscale structure derived from altimetry and to estimate their interannual variability. Indeed, the optimal currents are based on the synergy of the daily 1/8° Copernicus CMEMS altimeter-derived geostrophic velocities (data ID: SEALEVEL_MED_PHY_L4_REP_OBSERVATIONS_008_051) and the daily 1/24° CMEMS sea-surface temperatures for the Mediterranean Sea (data ID: SST_MED_SST_L4_REP_OBSERVATIONS_010_021). The optimal reconstruction method is based on the inversion of the ocean heat conservation equation in the mixed layer [15]. The principles of the optimal currents are thoroughly described in [15,20,21]. Such method takes advantage of the high-resolution spatial temporal gradients of the satellite-derived SST to improve the temporal (1 day) and spatial (1/24°) resolution of the altimeter derived geostrophic currents at the basin scale. The reconstruction method of the optimal currents yielded positive improvements for both the components of the motion in the SC [15].

- The Cross-Calibrated, Multi-Platform (CCMP) V2.0 ocean surface wind velocity which were downloaded from the NASA Physical Oceanography DAAC for the period July 1993 – May 2016 [22]. These products were created using a variational analysis method to combine wind measurements derived from several satellite scatterometers and microwave radiometers. The temporal resolution of the CCMP product is six hours, the spatial resolution is 25 km (level 3.0, first-look version 1.1).

Drifter velocities were divided in bins of 0.25°x0.25° and pseudo-Eulerian statistics were computed over the period 1993-2018 and qualitatively compared with the ADT derived from altimetry. The mean current field was also estimated in the period 2012-2016 using the optimal currents. The seasonal variability of the drifter, altimetry and optimal currents fields was estimated by dividing the dataset in two extended seasons: the extended summer corresponding to May-October, and the extended winter to November-April, as suggested by [9].

The CCMP six-hourly gridded analyses were used to quantify the wind stress and the vertical component of the wind stress curl $[curl\ \tau]_z$ over the study area:

$$\left[curl\tau\right]_z = \frac{\partial \tau_y}{\partial x} - \frac{\partial \tau_x}{\partial y}; \left(\tau_y, \tau_x\right) = \rho C_D \left(u_w, v_w\right) U_{10} \quad (1)$$

where (τ_x,τ_y) are the wind stress components, ρ (1.22 Kg/m^3) is the density of air, (u_w,v_w) and U_{10} are the components and the magnitude of the wind speed at 10 meters, respectively, and C_D is the drag coefficient already used in the Mediterranean Sea by [23,24]:

$$C_D = 10^{-3} \qquad \left|U_{10}\right| \le 3\frac{m}{s}$$

$$C_D = (0.29 + \frac{3.1}{U_{10}} + \frac{7.7}{U_{10}^2}) \times 10^{-3} \qquad 3\frac{m}{s} \le \left|U_{10}\right| \le 6\frac{m}{s} \quad (2)$$

$$C_D = (0.6 + 0.07U_{10}) \times 10^{-3} \qquad 6\frac{m}{s} \le \left|U_{10}\right| \le 26\frac{m}{s}$$

Wind stress and wind stress vorticity fields were used to speculate on the link between the wind variations and the seasonal and/or interannual variability of mesoscale structures.

Monthly means of the AGV and optimal currents fields were used to estimate the relative vorticity ($\boldsymbol{\zeta}$), defined as the vertical component of the velocity field curl:

$$\boldsymbol{\zeta} = \frac{\partial \boldsymbol{V}}{\partial \boldsymbol{x}} - \frac{\partial \boldsymbol{U}}{\partial \boldsymbol{y}}; \quad (3)$$

where U and V are the velocity components. The resulting current vorticity fields were spatially averaged in the regions of the main mesoscale structures listed in Table 1 and filtered (13-month moving average) in order to remove the seasonal and intra-annual variations.

3. Results

3.1 Mean currents and wind fields

The qualitative comparison between the ADT and drifter data shows that the two datasets fit rather well (Figure 2a), and allow us to update the pseudo-Eulerian current maps described in [9] and enhancing the schematic circulation maps published by [1] and [3] and summarized in Figure 1b. The averages were made over different periods in accordance with the availability of data: 1993-2018 for

156 the drifter and altimetry data (Figure 2a), 2012-2016 for the optimal currents (Figure 2b) and 1993-
157 2016 for the wind (Figures 2c, 2d). The time periods are rather long and the statistics rather robust to
158 consider the average in Figure 2a comparable with those in Figures 2c and 2d and representative of
159 the mean conditions in the SC. The optimal currents are available over a reduced period, and are
160 therefore not directly compared with the other datasets. They are rather used to bring out some
161 aspects of the current field that are not obvious using only drifters and altimetry data. The structures
162 emphasized in white in Figures 2a and 2b, are here described for the first time or with different shapes
163 and positions with respect to those schematized in Figure 1b.

164 **Table 1.** List of acronyms used in this paper

Geographical names	
SC	Sicily Channel
Water masses	
AW	Atlantic Water
LIW	Levantine Intermediate Water
Currents	
AC	Algerian Current
AIS	Atlantic Ionian Stream
ALC	Atlantic Libyan Current
ATC	Atlantic Tunisian Current
MIJ	Mid-Ionian Jet
BTC	Bifurcation Tyrrhenian Current
BATC	Bifurcation Atlantic Tunisian Current
TSC	Tyrrhenian Sicilian Current
Gyres and eddies	
ABV	Adventure Bank Vortex
ISV	Ionian Shelf break Vortex
LSBV	Libyan Shelf Break Vortex
MG	Medina Gyre
MCC	Maltese Channel Crest
MRV	Messina Rice Vortex
NSA	Northern Sicily Anticyclone
PV	Pantelleria Vortex
SCA	Sicily Channel Anticyclone
SG	Sidra Gyre
SISV	Southern Ionian Shelf break Vortex
SMG	Southern Medina Gyre
SMA	Southern Maltese Anticyclone
Physical properties	
ADT	Absolute Dynamic Topography
AGV	Absolute Geostrophic Velocities

The Atlantic Tunisian Current (ATC) originates from the branch of the Algerian Current (AC) that enters in the SC and flows southward between Pantelleria Island and the Tunisian coast [9]. It shows a complex pattern only partially described by the previous model studies. Indeed, the ATC splits in two branches at about 36.5°N (Figure 2a): one branch continues to move southward along the Tunisian coast (shown in white color), whereas another branch moves eastward south of Pantelleria Island. At about 35.5°N and 13°E the ATC splits another time: a part of the current forms the Bifurcation Atlantic Tunisian Current (BATC), the other part turns southward towards the Libyan coast at ~ 13°E. The latter branch describes the Atlantic Libyan Current (ALC; [1,3]), that move westward towards the Gulf of Gabes and eastward along the Libyan coast (Figures 1b, 2a).

Drifter and altimetry data confirm the well known meandering pattern of the Atlantic Ionian Stream (AIS) and outline the edge of the Maltese Channel Crest (MCC) located on the Maltese Plateau. The Medina Gyre (MG) is located on the west and/or southwest side of the Malta Island in agreement with the scheme of [3]. The region where the ATC splits and forms the BATC is characterized by a sudden reduction of depth due to the shelf extension (see the location of MG in Figure 1a) that probably facilitates the cyclonic rotation of the surface currents around 35°-36°N and 13°-14.5°E. It is interesting to note that [1] located the MG in a different position southeast of Malta (see Figure 2 of [1]). South of the MG, altimetry and drifter data detect another permanent cyclonic mesoscale structure that has never been described before in the literature; hereafter we will refer to this structure as the Southern Medina Gyre (SMG) (emphasized in white Figure 2a). The Libyan Shelf Break Vortex (LSBV) is well described only by altimetry data (Figure 2a) because of a scarce quantity of drifter tracks along the Libyan coast; this structure appears meridionally elongated and squeezed along the Libyan coast, showing a different shape and location with respect to [1].

The higher spatial resolution of the mean circulation derived by optimal currents (2012-2016; Figure 2b) permits a more detailed description of the mesoscale structure of the SC and the southern Tyrrhenian Sea. The anticyclonic structure, clearly visible along the northern coast of Sicily and located between the Aeolian Islands and Cape Gallo (38.1-38.5°N; 13.5-15°E), was observed by [25] in September 2012 but it was not described by these authors; hereafter it will be defined as the Northern Sicily Anticyclone (NSA). Another mesoscale anticyclone is located at the entrance of the SC (37.5-38°N; 11.5-12°E) and represents a kind of watershed between the waters entering the Tyrrhenian Sea (Bifurcation Tyrrhenian Current – BTC) and those entering the SC; hereafter we will define it as the Sicily Channel Anticyclone (SCA). A third mesoscale anticyclone is squeezed between the MG and Malta Island (35.5°-36° N; 14°-14.5° E) and we will define it hereafter as the Southern Maltese Anticyclone (SMA). Similarly, southeast of the Ionian Shelf break Vortex (ISV), there is another steady cyclonic structure hereafter defined as the Southern Ionian Shelf break Vortex (SISV). In addition, the optimal currents reveal new information on the shape of the Sidra Gyre (SG), which appears as a large anticyclone that involves two smaller anticyclonic structures (Figure 2b), and confirms the existence of the SMG (Figure 2b). The cyclonic circulation in the region of the Adventure Bank Vortex (ABV; 37-37.5°N; 12-13°E) is detected by the three datasets (drifter, altimetry and optimal currents) but the vortex is not well resolved by any of them; it appears more like a cyclonic meander rather than a vortex (Figure 2, upper panels).

In the study area the mean wind stress is oriented to the east in the southern Tyrrhenian Sea and to the southeast in the SC (Figure 2c) with amplitude (range of values between 0 and 0.04 Nm^{-2}) and directions in agreement with the results of [12]. The regions mostly impacted by the wind stress are located in the band north of 35°N and south of the southern Sicily coast (Figure 2c). The rotating motion induced by the wind (wind stress curl Figure 2d) is cyclonic (positive) along the southern and eastern Sicily coasts and on the Malta plateau, whereas it is anticyclonic (negative) along the Tunisia coast and in the southern Tyrrhenian Sea (along the northern Sicily coast). We can speculate that the wind field plays an important role in shaping the sub-basin circulation (e.g. the branch of the ATC that moves southward along the Tunisia coast) and in defining the sense of rotation of the mesoscale

structures located around the Sicily coast (e.g. the ABV, the Messina Rise Vortex -MRV, the ISV and the NSA).

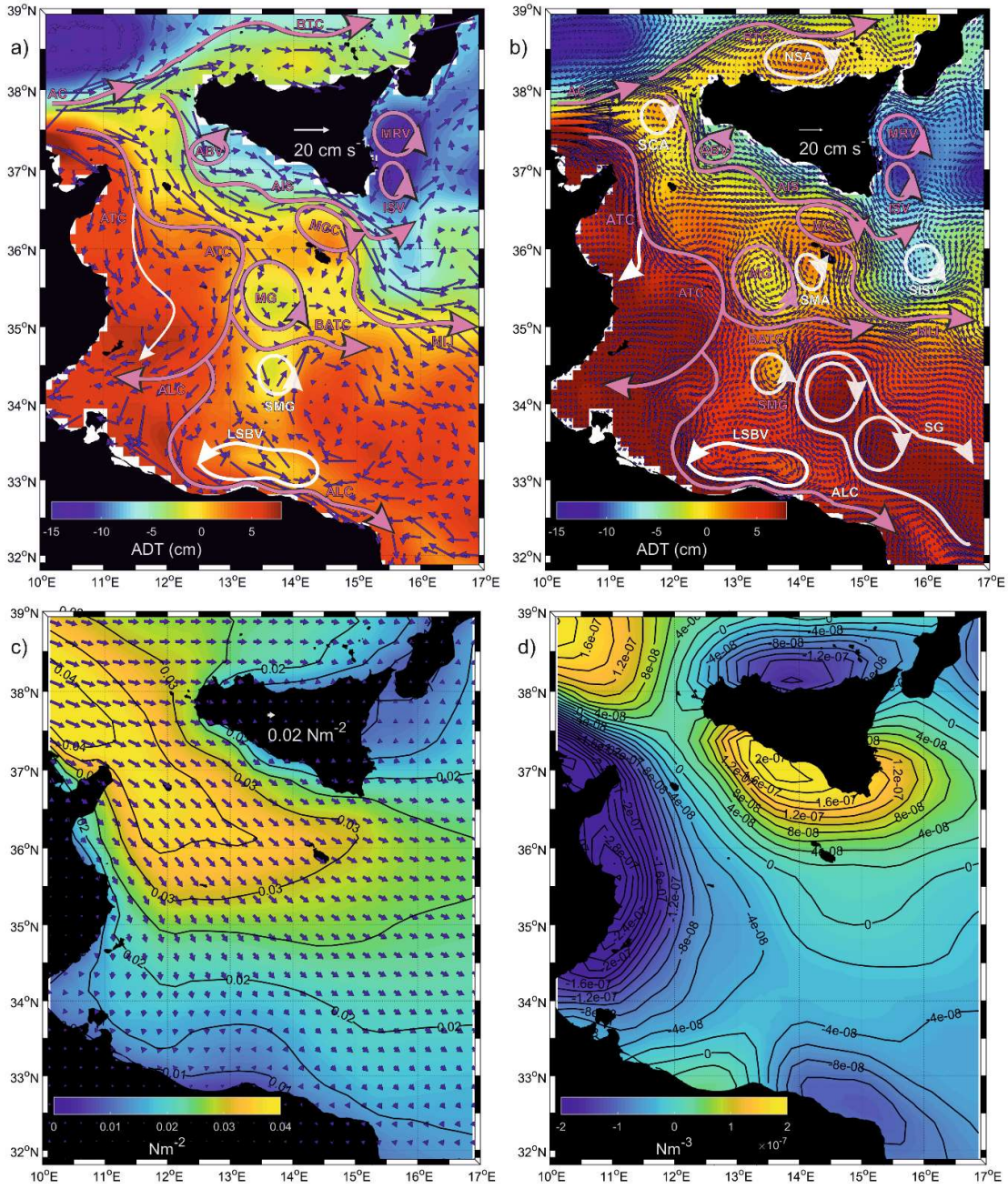

Figure 2. Mean drifter currents (a) in spatial bins of 0.25°x0.25° (blue vectors) superimposed on mean maps of absolute dynamic topography (colours) during the period 1993-2018; mean optimal currents (b) in spatial bins of 1/12° (vectors; one vector every two grid point is plotted) superimposed on mean maps of absolute dynamic topography (colours) during the period 2012-2016. The structures emphasized with white arrows in panels (a) and (b) are new or with different shapes and positions with respect to those described in Figure 1b; the structures already known are highlighted with pink arrows. (c) Mean map of the wind stress amplitude (colours) and direction (vectors) and (d) wind stress curl over the period 1993-2016.

226 *3.2 Seasonal variability of currents and wind fields*

227 The seasonal variability of the drifter-derived and optimal current fields is shown in Figure 3 together
228 with the altimetry data. Results substantially confirm the paths described in [9], but add new insights.
229 The BTC is a permanent feature as shown by [1], and it is stronger in winter (Figures 3b and 3d;
230 winter speeds larger than 20 cm/s; mean summer speeds of ~ 10 cm/s), whereas the NSA is much
231 more intense in summer (Figures 3a and 3c; mean winter speeds of ~ 5 cm/s; mean summer speeds of
232 ~ 10 cm/s). Along the northern coast of Sicily the drifter data describe a westward current during
233 summer, with the consequent inflow of surface water in the SC (Figure 3a), whereas the coastal
234 currents moves eastward during winter (Figure 3b). This summer westward current (mean speeds of
235 ~ 10 cm/s) was already described in [3] and defined as the Tyrrhenian Sicilian Current (TSC). The TSC
236 is not identified by the optimal currents (Figures 3c and 3d).

237 The ATC is part of the permanent pattern of the SC, in agreement with [3] and it is more intense and
238 more meandering in nature during the extended winter (Figures 3b, 3d; maxima winter speeds of ~
239 30 cm/s; maxiama summer speeds of ~ 20 cm/s); it is interesting to note that [1] described it as a winter
240 structure. The cyclonic Pantelleria Vortex (PV) is observed only during the extended winter (Figures
241 3b, 3d; speeds of 10-15 cm/s), in agreement with the optimal currents and with [3] and in
242 disagreement with [1], that describe this as part of the permanent pattern. The MCC is stronger
243 during the extended summer (speeds larger than 15 cm/s), as well as the AIS (Figures 3a, 3c; mean
244 winter speed of ~ 5 cm/s; mean summer speeds of ~ 15 cm/s). The SG is stronger and larger in size
245 during summer (Figures 3a and 3c; mean winter speeds of ~ 7 cm/s; mean summer speeds of ~ 12
246 cm/s; winter longitudinal extension of ~ 100 km; summer longitudinal extendion larger than 250 km),
247 in agreement with the results of [26] that report the SG seasonal expansion in summer and contraction
248 in winter. The ISV and the MRV are permanent structures, in agreement with [1], and they are
249 stronger in winter (Figures 3b, 3d; mean winer speeds of ~ 9 cm/s; mean summer speeds of ~ 6 cm/s);
250 also the SISV is a permanent structure more intense in winter, according to the optimal currents
251 (Figures 3d; mean winer speeds of ~ 10 cm/s; mean summer speeds of ~ 5 cm/s). The BATC is
252 predominant during winter south of the MG (Figures 3b and 3d; maxima winer speeds of ~ 20 cm/s;
253 maxima summer speeds of ~ 10 cm/s), in agreement with [1]. The ALC is stronger in winter (Figures
254 3b and 3d; speeds larger than 15 cm/s), whereas the LSBV is stronger in summer (Figures 3a, 3c;
255 speeds larger than 25 cm/s).

256 The wind stress and the wind stress curl are more intense in winter (Figure 4) influencing the seasonal
257 variability of some sub-basin currents such as the BTC, the ALC, the BATC; the winter intensification
258 of the BATC and its interaction with the topography lead to an intensification of the MG. The wind
259 stress does not impact the circulation structures which are more intense in summer (MCC, AIS, NSA,
260 SG), when the wind stress and the wind stress curl are weakened. The seasonal variability of these
261 structures is presumably related to other forcings such as the instability of the surface currents and
262 the interaction with the topography. The behaviour of the AIS and of the MCC confirms this insight:
263 the AIS is stronger in summer (Figure 3a), when the wind stress is weaker (Figure 4a) and its meander
264 on the Malta Plateau (the MCC) is anticyclonic, although the vorticity induced by the wind in this
265 region is substantially cyclonic (Figure 4c). Along the northern coast of the Sicily, the amplitude of
266 the wind stress and the anticyclonic vorticity induced by the wind are stronger in winter (Figure 4),
267 whereas the strengthening of the NSA is observed in summer (Figures 3a and 3c). This result suggests
268 that the wind influences the sense of rotation of the surface circulation in the NSA, but other forcings
269 modulate the strength of the seasonal and interannual variability of this circulation structure. The
270 summer intensification of the LSBV appears to be instead related to the intensification of the cyclonic
271 wind stress curl along the western Libyan coast (Figure 4c). The SG shows a pronounced longitudinal
272 extension in summer (Figure 3a), when the wind stress is weaker but the vorticity induced by the
273 wind is essentially anticyclonic in the southeastern region of the SC (Figure 4a); its southern margin
274 is oriented parallel to the Libyan coast following the 400 m isobath.

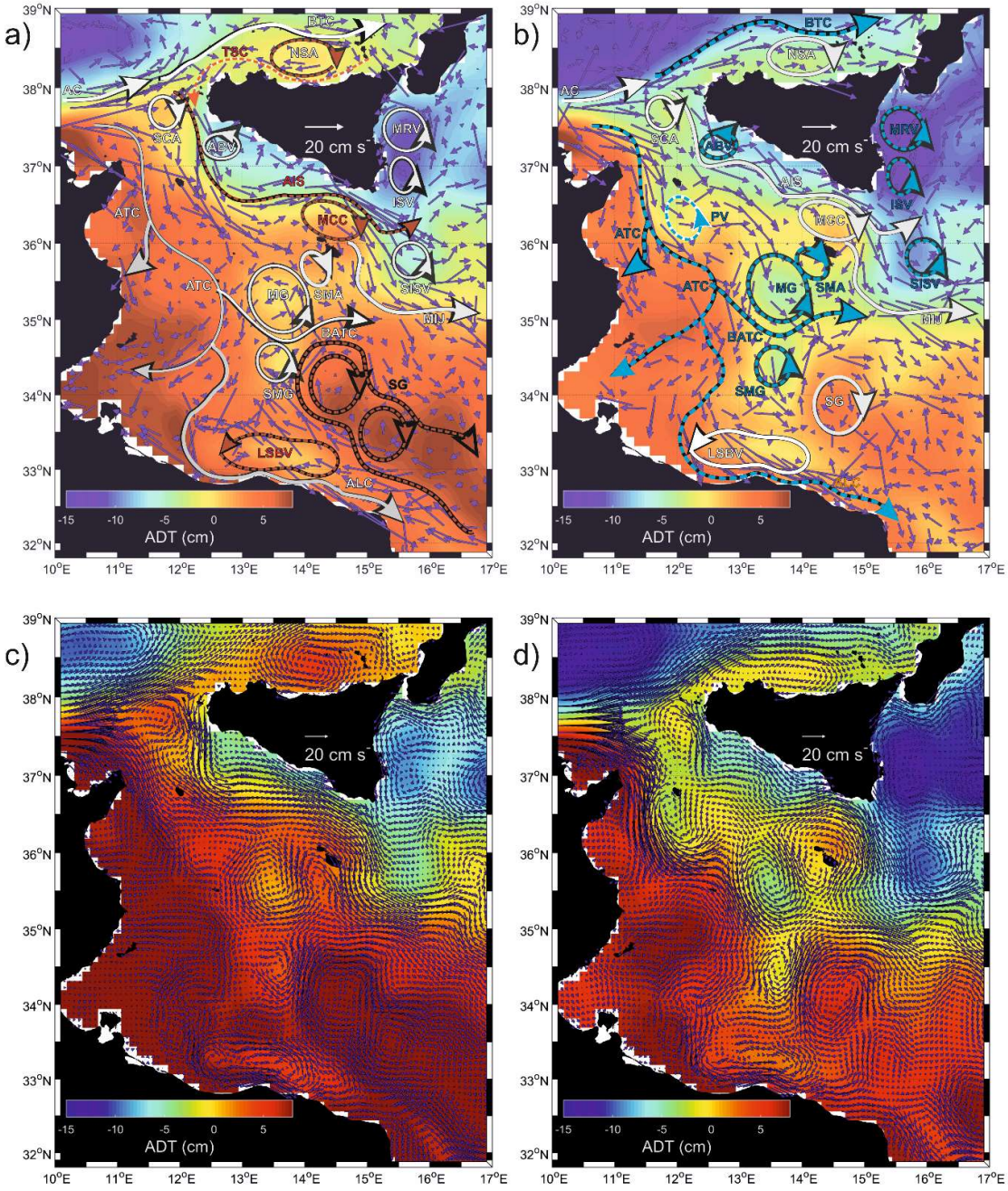

Figure 3. Pseudo-Eulerian drifter statistics (blue vectors) superimposed on mean maps of the absolute dynamic topography (colours) for the (a) extended summer and (b) extended winter. The schematic circulation structures superimposed on the currents field are coloured with red arrows (a) when they are most intense in summer and with light blue arrows (b) when they are most intense in winter. Mean optimal currents in spatial bins of 1/12° (blue vectors: one vector every two grid point is plotted) superimposed on mean maps of absolute dynamic topography (colours) during the period 2012-2016 for the (c) extended summer and (d) extended winter.

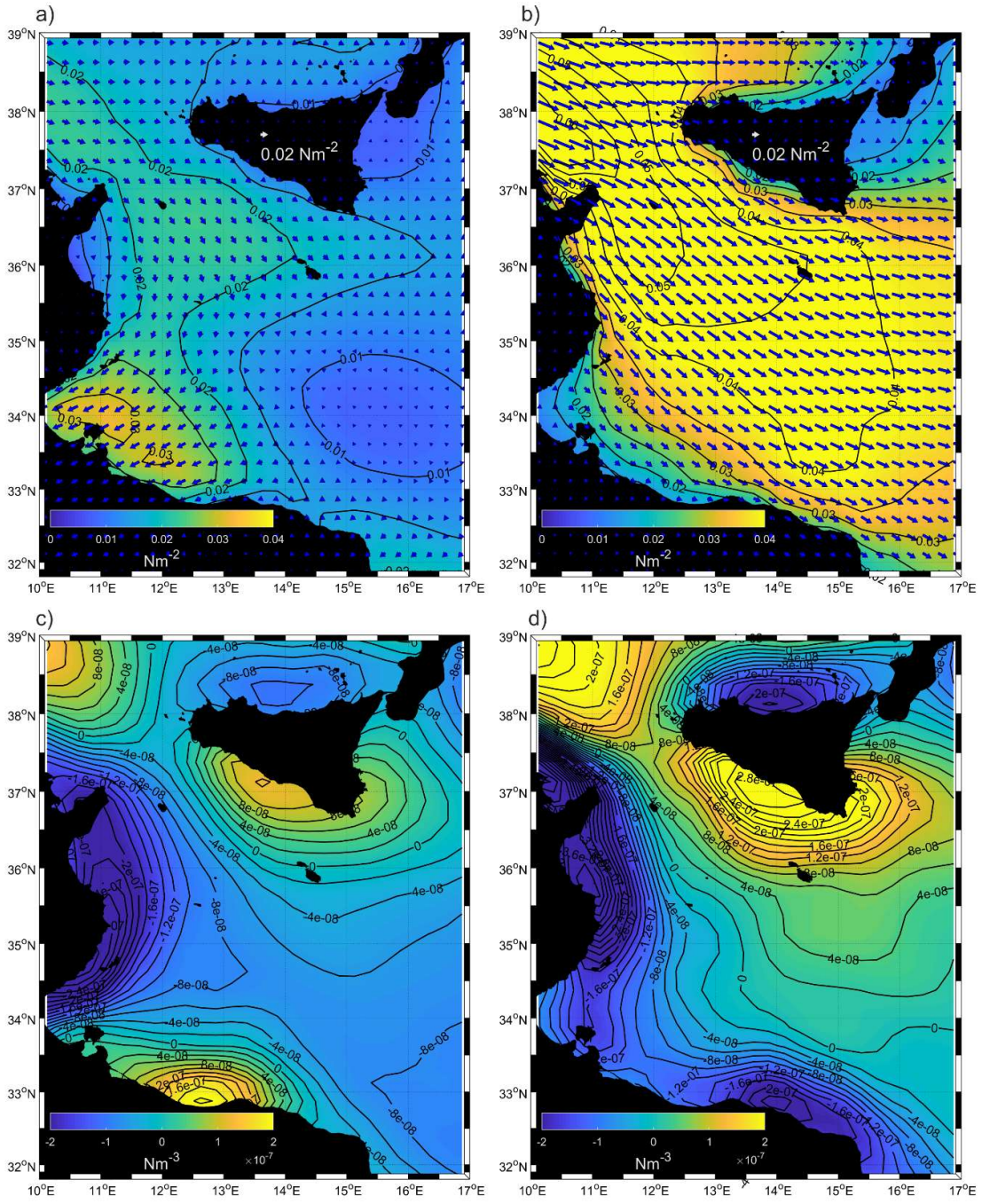

Figure 4. Mean map of the wind stress (upper panels) amplitude (colours) and direction (vectors) and (d) wind stress curl (lower panels) over the extended summer (a, c) and extended winter (b, d).

3.3 Decadal variations

Decadal variations are emphasized by removing the mean ADT and AGV (1993-2018) fields from the interannual composite mean over the time periods characterised by the anticyclonic (1993-1996, 2006 – 2010 and 2016-2017) and cyclonic (1997-2005 and 2011 – 2016) circulation modes in the northern Ionian (Figure 5). In the region located between Pantelleria and Malta islands (35.5°N-37°N, 11°E-15°E), the surface currents are samller than the mean field during the anticyclonic mode (Figure 5a; current anomalies are oriented in an opposite direction with respect to the mean field) and larger

during the cyclonic mode (Figure 5b). Along the northern coast of the Sicily, the NSA is reduced in intensities with respect to the mean field during the anticyclonic mode (Figure 5a; the current anomalies are oriented ciclonically) and increased during the cyclonic mode.

The largest variations are observed east of 15°E, in agreement with the results of [24]. The MRV and the SISV are less intense than the mean currents during the anticyclonic mode (Figure 5a) and slightly more intense during the cyclonic mode (Figure 5b). The AIS tends to be deflected towards the northern Ionian during the anticyclonic circulation mode (northeastward currents along the Sicily eastern coast) and the MIJ is reduced in intensity with respect to the mean currents (Figure 5a). During the cyclonic circulation mode the AIS feeds the MIJ, that shows larger intensities with respect to the mean, and the currents are mainly directed southwestward along the western coasts of the Ionian Sea (Figure 5b).

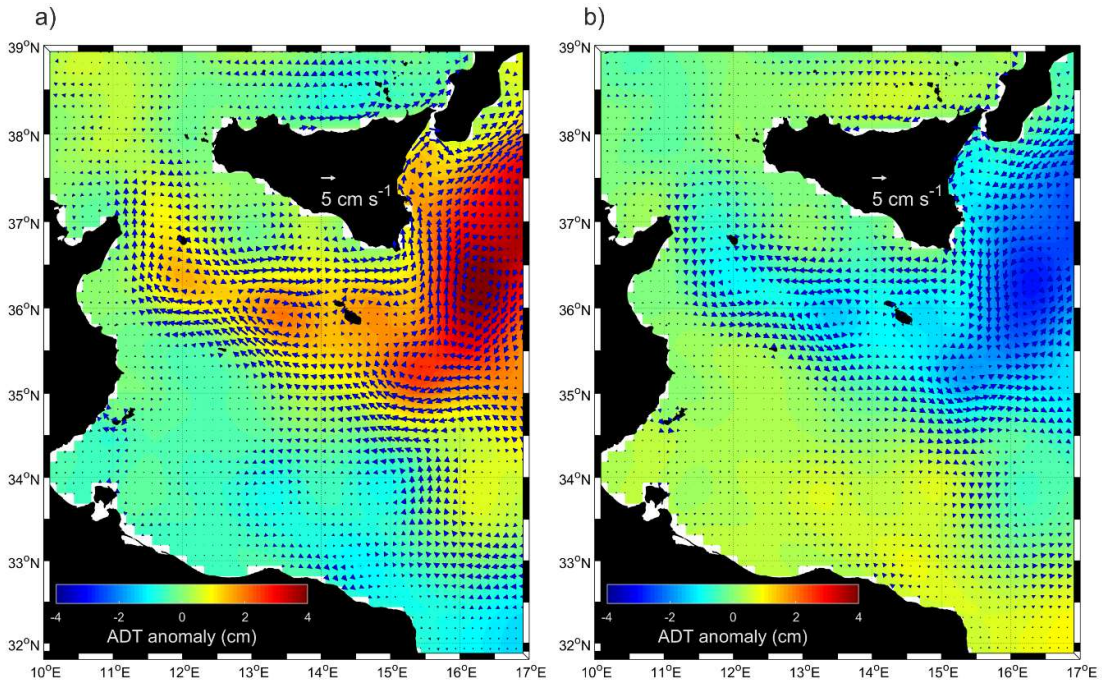

Figure 5. Mean maps of absolute geostrophic velocity anomalies (vectors) superimposed to the absolute dynamic topography anomalies (colours) during a) anticyclonic (1993-1996, 2006-2010, 2017-2018) and b) cyclonic (1997-2005 and 2011-2016) circulation modes in the northern Ionian.

3.4 Interannual variability and vertical structure of the quasi-permanent mesoscale eddies in the Sicily Channel and southern Tyrrhenian Sea

The main quasi-permanent mesoscale eddies of the SC and southern Tyrrhenian are analysed in term of their interannual variability, using the time series of spatially averaged vorticity fields derived both from altimetry and optimal currents data. In the period in which the optimal currents are available the accuracy of the vorticity derived by the AGV is generally improved, showing larger complexity in the temporal variability of the signal (see Figures 6, 8, 11). The thermohaline properties and the vertical extension in the water column of these mesoscale eddies is studied using the Argo float profiles.

3.4.1 Southern Tyrrhenian Sea and Sicily Channel entrance

The analysis of the vorticity field in the areas of the NSA (38.1-38.5°N; 13.5-15°E) and SCA (37.5-38°N; 11.5-12°E) confirms that the anticyclonic nature of these regions persists with time (Figure 6). A more

accurate analysis of the temporal evolution of the vorticity in the NSA shows quasi-decadal variations of the intensity of the vorticity field that coincide with the inversions of the surface circulation in the northern Ionian. The black dashed lines in Figure 6 give an indication of the mean vorticity values during each anticyclonic/cyclonic circulation mode. The anticyclonic vorticity of the NSA is reduced during the anticyclonic circulation modes of the northern Ionian (1993-1996, 2006-2010, 2017-2018), whereas it is enhanced during the cyclonic circulation modes (1997-2005, 2011-2016). This result supports the relationship suggested by [27] between the large–scale interior ocean variability in the central Mediterranean Sea and the local dynamics. More specifically, these authors suggest a link between the inversions of the surface circulation in the northern Ionian and the local tidal observations in the area of the Strait of Messina. The present work shows that not only the Strait of Messina, but all the coastal area adjacent to the northern Sicily coast, can be influenced by the variability attributed to the large scale dynamics of the central Mediterranean.

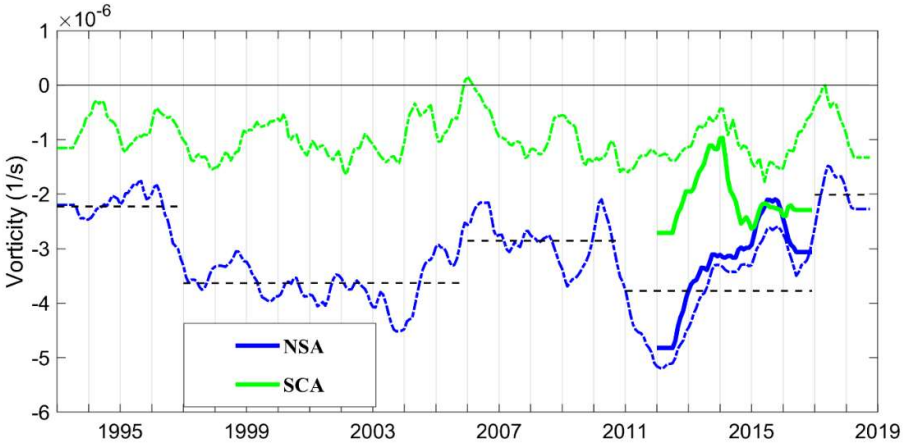

Figure 6. Time series of the spatially averaged, low pass filtered (13-months) vorticity field over the regions of the NSA and SCA. Dashed-dotted lines are referred to the vorticity field derived from the AGV; Continuous lines are related to the vorticity field derived from optimal currents in 2012-2016. Dashed black lines show the average values of the vorticity over each anticyclonic/cyclonic period of the Northern Ionian Gyre.

The vertical structure of the NSA is defined by the profiles of the float WMO 6900981 that circulates on the border of the NSA between late April 2012 and early January 2013 (Figures 7a and 7b). This float shows that the NSA extends about 50 m in depth and confirms its anticyclonic nature with a reduction of density and the deepening of the isopycnal surfaces, in particular between the end of June 2012 and November 2012 when the float profiles were close to the core of the eddy. The trajectory of the float WMO 6900981 gives an indication of the intermediate current displacements at the parking depth (350 m; see Table 2). It is interesting to note that the intermediate currents in the region of the NSA, during the period covered by the float WMO 6900981, flow in an opposite direction (cyclonic displacements; Figure 7a) with respect to the mean surface currents (Figure 2b). The diagram in Figure 7b shows a gap of the float profiles between 1 September 2012 and 20 October 2012. Despite this gap, the float remains confined to the eastern part of the NSA, from which it moves away only in December 2012. Unfortunately, we have no floats entrapped in the SCA.

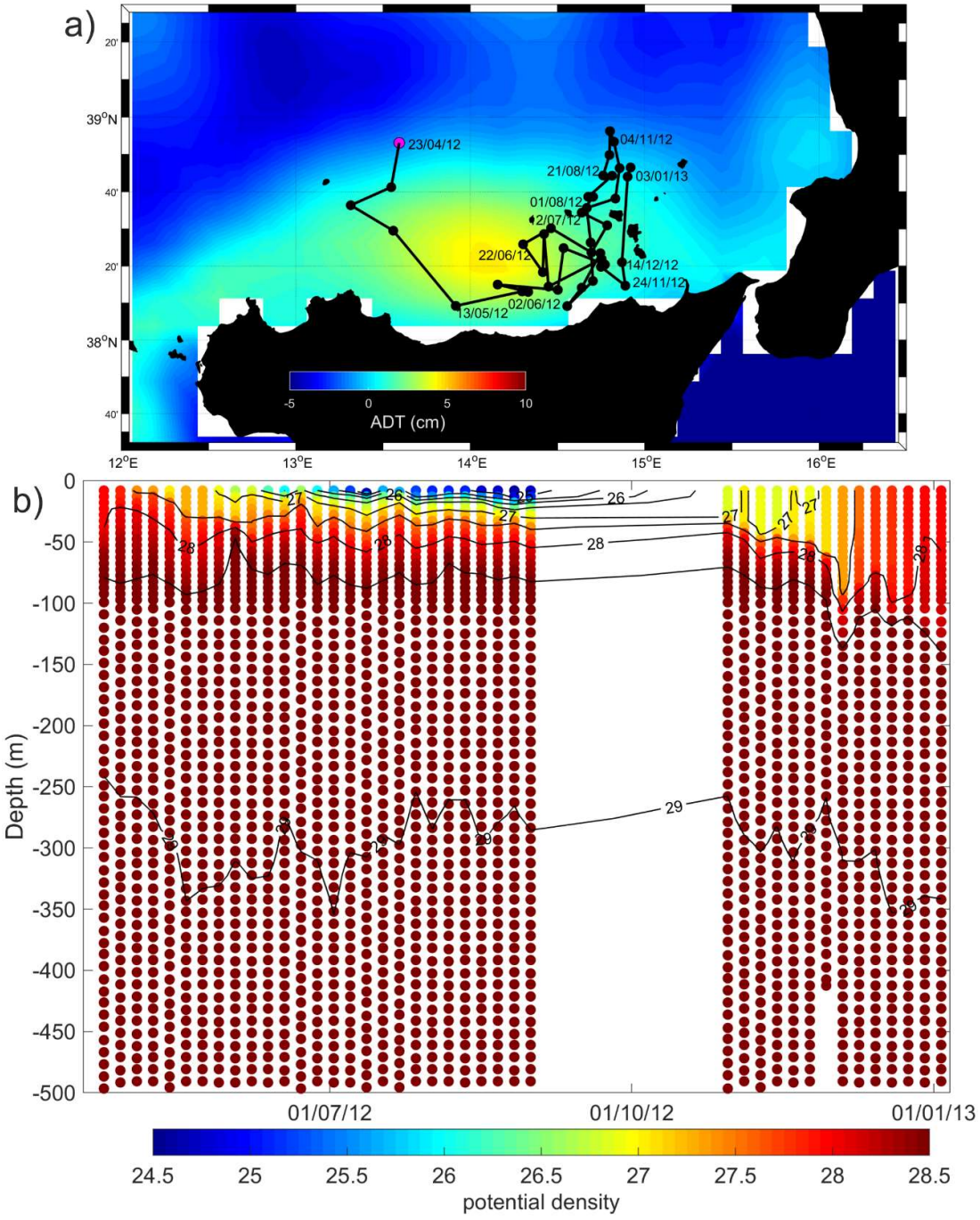

Figure 7. Map of the trajectory (black line) and profile positions (first profile: magenta dot; other profiles: black dots) of the float WMO 6900981 superimposed on the mean map of the ADT (between 18-Apr-2012 and 3-Jan-2013) (a), and contour diagram of the potential density versus depth and time (b).

3.4.2 Malta plateau

The surface circulation in the region of the Malta Plateau is strongly influenced by the flow of the AIS that forms a large anticyclonic meander defined as MCC. The permanent anticyclonic vorticity in this region (36.1-36.8°N; 14-15°E) is confirmed by the time series of vorticity field (Figure 8). At local scale, this meander can sporadically create an anticyclonic gyre on the Malta plateau [28].

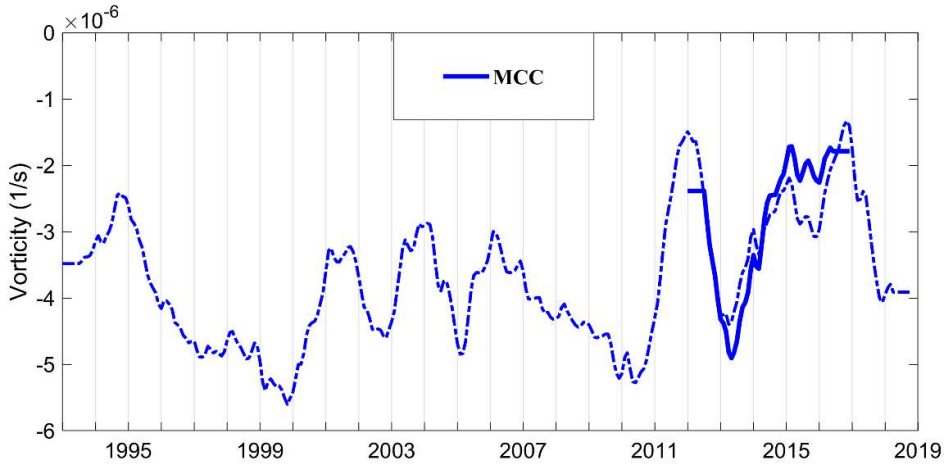

Figure 8. Time series of the spatially averaged, low pass filtered (13-months) vorticity field over the regions of the Malta plateau. Dashed-dotted lines are referred to the vorticity field derived from the AGV; continuous lines are related to the vorticity field derived from optimal currents in 2012-2016.

In the framework of the Italia-Malta Calypso Project [28], about 38 drifters were deployed on the Malta plateau between December 2012 and September 2016. These drifters were captured by the anticyclonic gyre on the plateau in two specific deployments: December 2012 and March 2014 (Figure 9). In December 2012-January 2013, drifters are captured by the anticyclonic gyre for about four weeks (approximately between 14 December 2012 and 10 January 2013) before being transported out of the plateau (Figure 9a). This gyre is also confirmed by the trajectory of the float WMO 6901044 (Figure 10a) and by HF radar measurements [29]. On 22 March 2014, six drifters were deployed in the area and were trapped in the gyre for about 2 weeks (Figure 9b). Drifters allow to estimate the radius and the rotation period of the structure considering the centroids computed from all the closed loops of the drifter trajectories. The radius spanned between 11 and 27 km and the period increased from 4.1 to 8.4 days, in coincidence with an increasing the distance from the centre.

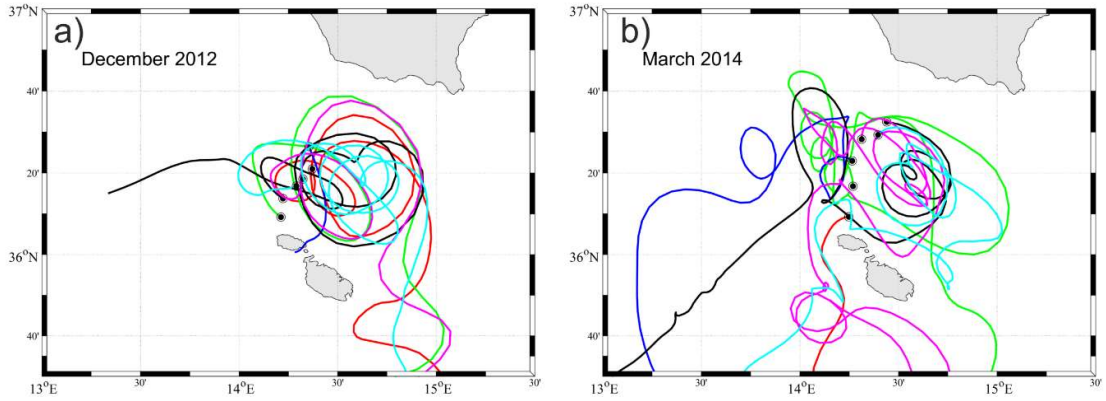

Figure 9. Trajectories and deployment positions (black dots) of the drifters deployed on the Malta Plateau in December 2012 (a) and March 2014 (b).

The float WMO 6901044 was entrapped in the MCC between 15 December 2012 and 17-February-2013, then it joined a cyclonic structure located north-western of the Malta Plateau (Figures 10a). It had a cycling period of 1 day, and its trajectory gives an indication of the 350 m displacements (see Table 2). In the first part of its tracks, the float sampled the interior of the anticyclonic MCC showing a deepening of the isopycnal surfaces (December 2012-January 2013) and reduced densities; in February 2013 the float moved along the border of the MCC, then it was entrapped in the cyclonic

structure located in the north-western proximities of the Malta plateau (Figure 10b). Both the MCC and the cyclonic structure show a similar vertical structure, extending to a depth of about 200 -250 m (Figure 10b).

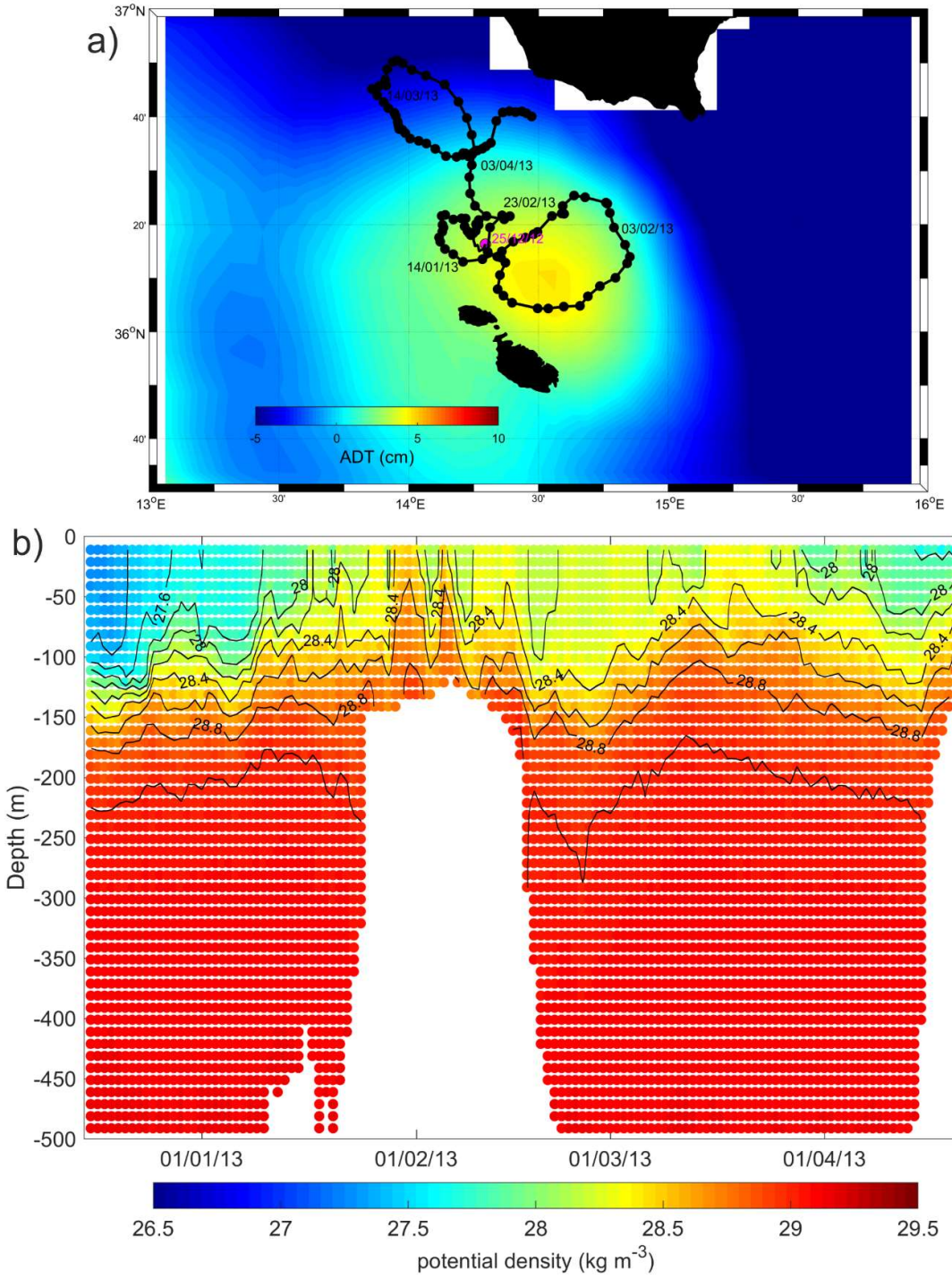

Figure 10. Map of the trajectory (black line) and profile positions (first profile: magenta dot; other profiles: black dots) of the float WMO 6901044 superimposed on the mean map of the ADT (between 16-Dec-2012 and 30-April-2013) (a), and contour diagram of the potential density versus depth and time (b).

3.4.3 South of Malta

The time series of the vorticity fields obtained at the locations of the mesoscale eddies south and south-west of Malta are shown in Figure 11. The MG (35°-35.5°N; 13°-14°E) and the SMA (35.5°-36°N; 14°-14.5°E), two adjacent structures located south-west of the Maltese Islands, show larger variabilities of the vorticity field with respect to the SMG (34°-35°N; 13°-14°E) and LSBV (33°-33.5°N; 12.5°-14°E). This behaviour is probably related to the wind-stress, which is more intense in the Malta region than in the southern SC (Figure 2c). The vorticity of SMA increases with time over the considered period.

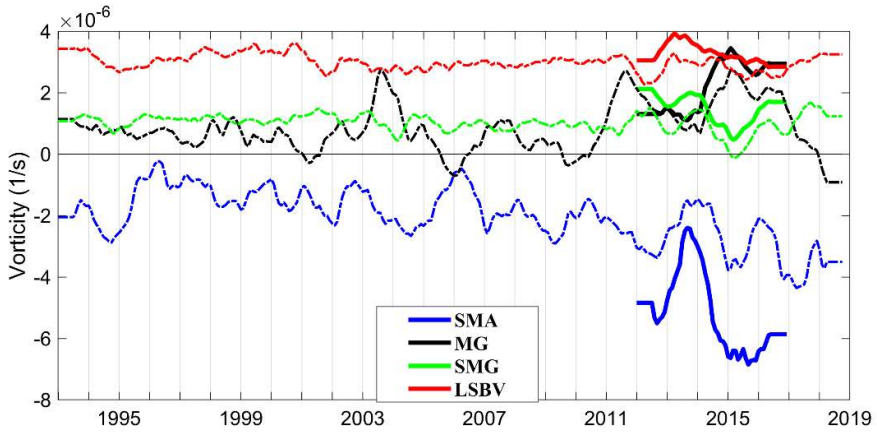

Figure 11. Time series of the spatially averaged, low pass filtered (13-months) vorticity field over the regions of MG, SMA, SMG and LSBV. Dashed-dotted lines are referred to the vorticity field derived from the AGV; continuous lines are related to the vorticity field derived from optimal currents in 2012-2016.

The float WMO 6903242, became entrapped in the anticyclonic SMA in mid-September 2018, therefore describes five loops around the eddy core before being captured by the eastward BATC (Figure 12a). It had a short cycling period (see Table 2) and its trajectory indicates the mean near surface displacements (0-180 m). The subsurface density distribution clearly shows the net differences between the water masses located east (potential density smaller than 24.8 kg/m^3) and south (potential density larger than 26 kg/m^3) of the of SMA (Figure 12b). The SMA extends down to a depth of about 40 m (Figure 12c). At the end of October 2018 the float left the cyclonic structures and moves eastward encountering surface waters of eastern origin, denser than 1026 kg/m^3.

Table 2. *List of selected Argo float with dates and positions of the first and the last profile considered in this work, parking and profiling depths and the cycle period of each instrument.*

Float WMO	First profile	Last profile	Parking depth (m)	Profile depth (m)	Cycle Period (days)
6900981	23-Apr-2012 38.9°N, 13.6°E	3-Jan-2013 38.8°N, 14.9°E	350	600/2000	5
6901044	16-Dec-2012 36.3°N, 14.3°E	22-Apr-2013 36.7°N, 14.5°E	350	700	1
6903242	11-Sep-2018 35.4°N, 14.4°E	13-Nov-2018 35.2°N, 15.0°E	200	200	0.125
1900629	22-Aug-2007 33.7°N, 13.5°E	05-Mar-2008 34.5°N, 13.9°E	350	700/2000	5
1900948	19-Jul-2015 33.0°N, 15.6°E	28-Feb-2016 32.9°N, 15.0°E	1000	1500	4
1900954	16-Oct-2016 35.8°N, 15.6°E	05-Mar-2017 35.2°N, 14.8°E	1000	1500	4

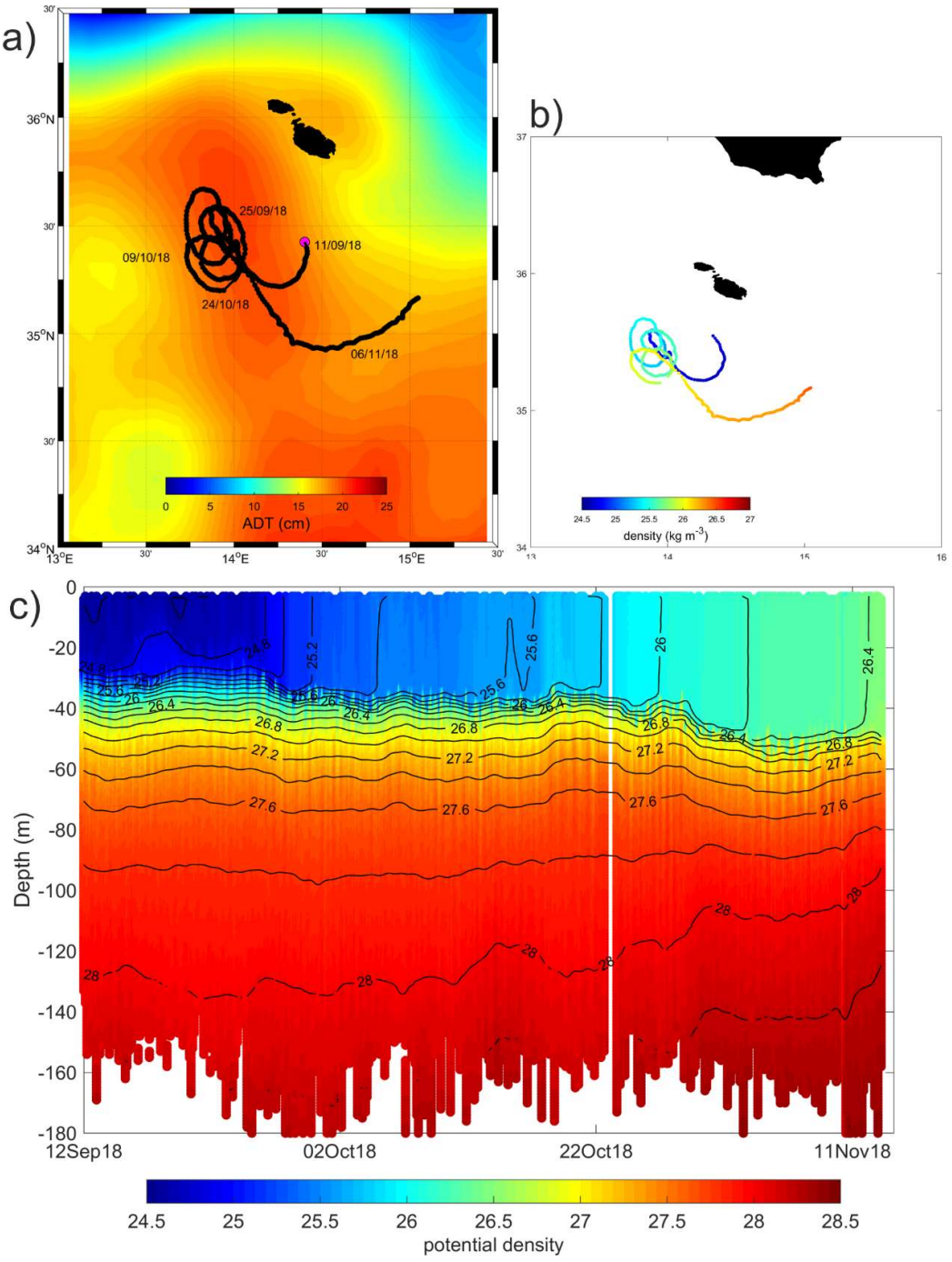

Figure 12. Map of the trajectory (black line) and profile positions (first profile: magenta dot; other profiles: black dots) of the float WMO 6903242 superimposed on the mean map of the ADT (between 12-Sep-2018 and 11-Nov-2018) (a), map of the potential density measured at 20 m depth (b), and contour diagram of the potential density versus depth and time (c).

The float WMO 1900629, coming from the Libyan coast, was entrapped in the cyclonic SMG at the end of 2007 (Figure 13a). This structure is denser than the surrounding waters (Figure 13b). Since in the region of the SMG the maximum depth of the sea bottom is of about 400 m (Figure 1a), and since the cyclonic trajectory of the float WMO 1900629 (Figure 13a) represents the displacements of the currents at the parking depth of 350 m (see Table 2), we can conclude that the cyclonic structure affects the entire water column in this area.

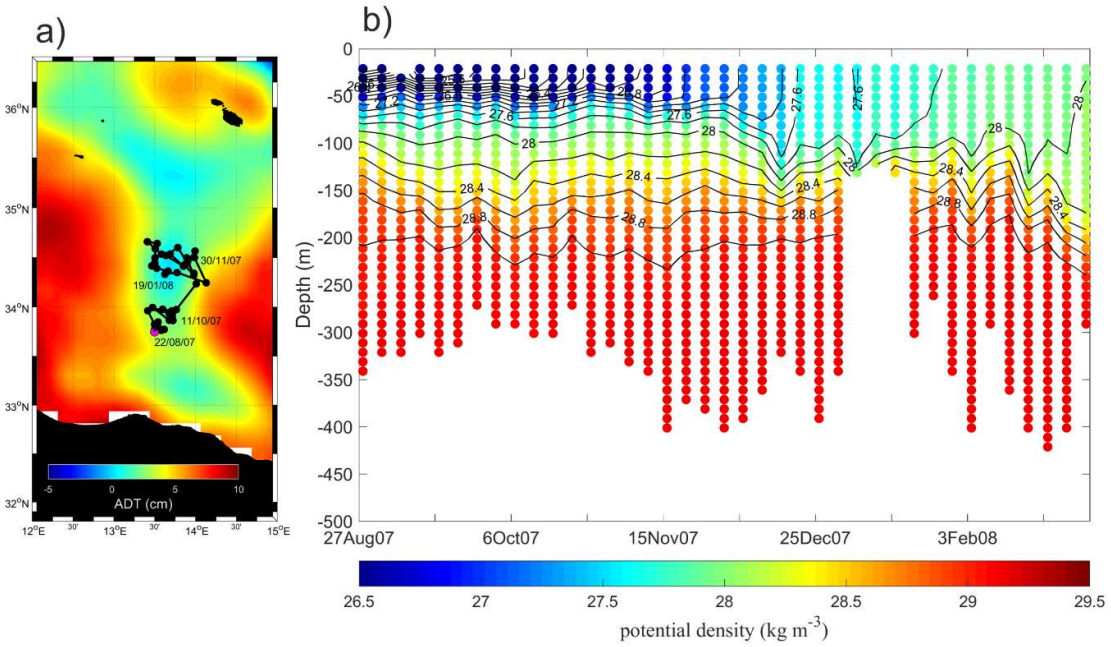

Figure 13. Map of the trajectory (black line) and profile positions (first profile: magenta dot; other profiles: black dots) of the float WMO 1900629 superimposed on the mean map of the ADT (between 27-Aug-2007 and 23-Feb-2008) (a), and contour diagram of the potential density versus depth and time (b).

The cyclonic LSBV is sampled by the float WMO 1900948 during the period October 2015 – February 2016 (Figure 14a). The entrance of this float in the LSBV is emphasized in Figure 14b by higher density compared to the surrounding waters, and by changes in the shape of the isopycnal surfaces. Even if the float WMO 1900948 has a parking depth of 1000 m (see Table 2), its displacements represent the current at 350 m depth due to the bathymetry of the LSBV region (see Figures 1a and 14b). We can conclude that the cyclonic structure affects the entire water column in this area (Figure 14b).

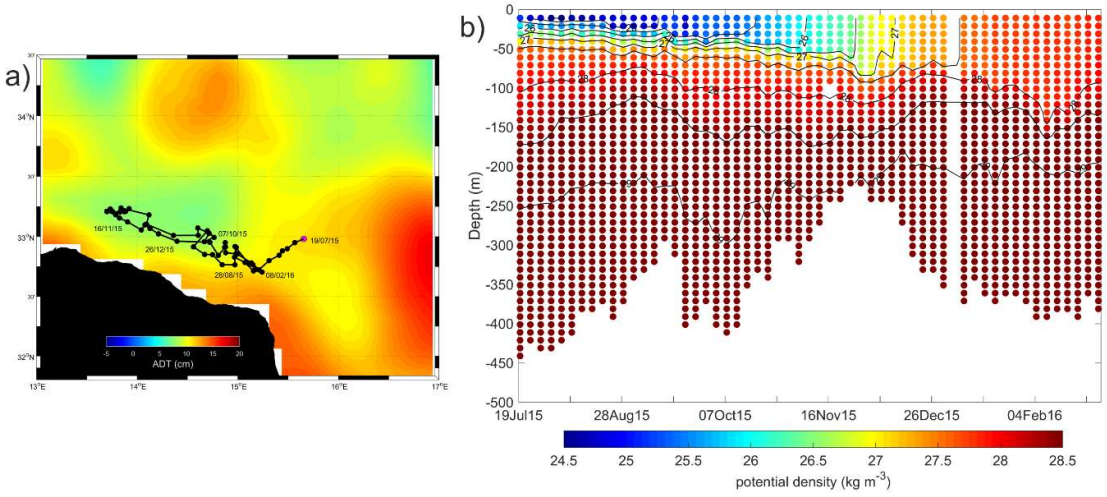

Figure 14. Map of the trajectory (black line) and profile positions (first profile: magenta dot; other profiles: black dots)of the float WMO 1900948 superimposed on the mean map of the ADT (between 19-Jul-2015 and 28-Feb-2016) (a), and contour diagram of the potential density versus depth and time (b).

3.4.4 Ionian cyclones

Figure 15a shows the time series of the vorticity field along the eastern coast of Sicily (MRV and ISV area – 36.5°-38°N; 15°-16°E) and in the region of the SISV. Figure 15a show an inconsistency between the vorticity derived from AGV and those derived from the optimal currents in the region of the SISV. From the optimal currents validation carried out by [15], this structure lies in an area where the method degrades the quality of the surface currents (in particular of the meridional component) when compared with the AGV(see Figure 10 of [15]). Therefore the optimal currents could not be consistent in the description of SISV.

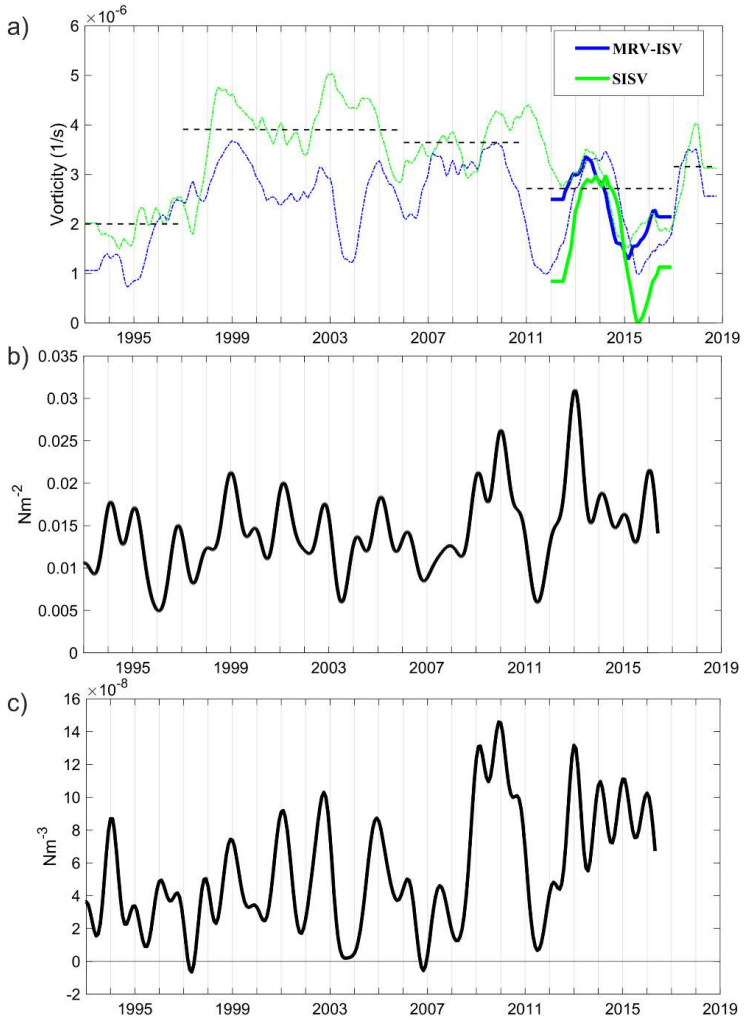

Figure 15. a) Time series of the spatially averaged, low pass filtered (13-months) vorticity field over the regions of the MRV-ISV and SISV. Dashed-dotted lines are referred to the vorticity field derived from the AGV; continuous lines are related to the vorticity field derived from optimal currents in 2012-2016; b) time series of the monthly, spatially averaged low-pass filtered (13-months) wind-stress and c) wind stress vorticity in the MRV region.

The MRV and ISV are wind-driven structure [7,24] and their interannual variability is related to the wind-stress along the eastern coast of Sicily (Figures 15b and 15c): e.g. lower values of current vorticity in the MRV-ISV regions are related to lower wind-stress and lower wind stress curl. The SISV (35.5°-36.6°N; 15°-16°) is not influenced by the wind-stress vorticity, whereas it appears to be influenced by the quasi-decadal reversal of the northern Ionian (see black dashed lines in Figure 15a

that give an indication of the mean vorticity value during each anticyclonic/cyclonic circulation mode) in the period 1993-2010. After 2010, the vorticity of the currents is no longer consistent with the decadal variability and seems to be rather linked to some other phenomena, that currently are not detectable from our datasets.

The float WMO 1900954, coming from the eastern Ionian, was entrapped in the SISV in December 2017 (Figure 16a) and shown an increase of density with respect to the water located north of this mesoscale structure (Figure 16b). Even if the float WMO 1900954 has a parking depth of 1000 m (see Table 2), its displacements represent the current at about 500 m depth due to the bathymetry of the SISV region (see Figures 1a and 16b). The vertical extension of the SISV is about 100 m (Figure 16b).

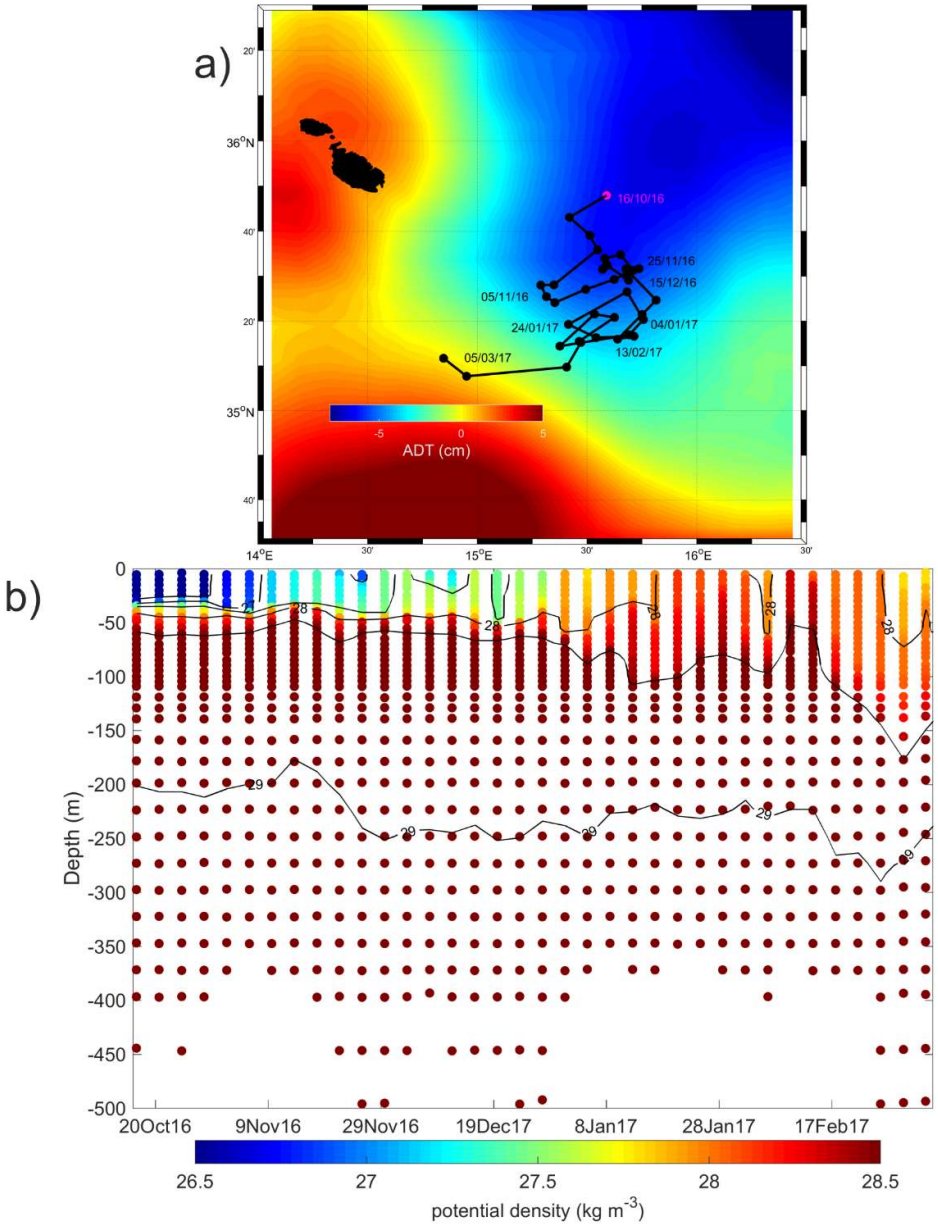

Figure 16. Map of the trajectory (black line) and profile positions (first profile: magenta dot; other profiles: black dots) of the float WMO 1900954 superimposed on the mean map of the ADT (between 20-Oct-2016 and 7-Mar-2017) (a), and contour diagram of the potential density versus depth and time (b).

4. Discussion and Conclusions

The main findings of this work are summarized in Figure 17, where a schematic diagram of the surface circulation, based on the mean circulation map depicted in Figure 2b, is presented. In Figure 17a the main circulation structures are classified according to their seasonal variability, whereas in Figure 17b they are identified based on the main forcing factor that determines them.

The basin scale circulation is essentially oriented according to the wind stress direction (northwest – southeast; Figures 2a, 2c, 17). Most of the main sub-basin scale current systems and mesoscale structures are permanent but affected by a strong seasonal variability (Figure 17a); only the TSC and the PV show a seasonal incidence and occur exclusively in summer and winter, respectively. The BTC, ATC, BATC and ALC show a winter intensification (Figure 17a) concurrent with the intensification of the wind stress (Figures 3 and 4); for this reason they are classified as wind-driven features in Figure 17b. The relationship between the sub-basin scale structures and the wind stress variability was already suggested by [13,30]. Other sub-basin scale and mesoscale structures - e.g. the meandering AIS, the SG, and the MCC - are stronger in summer, when the wind stress is weaker. Hence, we exclude the direct impact of the wind on the variability of these structures. Rather, we suggest that they are influenced by other forcings such as the instability of the surface currents and/or their interaction with the complex and relative shallow bottom topography (Figure 17b), characterised by continental shelves and channels.

The MG and SMA are located in a highly dynamic region (high level of Eddy Kinetic Energy, see Figure 6 of [24] and Figure 9a of [11]) characterized by the split of the ATC, whose eastward branch forms the BATC, and by a sudden reduction of depth (Figure 1a). These factors probably interact in facilitating the eddies formation and retention. From these considerations, the MG and SMA are influenced by the surface current dynamics and/or topography (Figure 17b). They are stronger in winter because the sub-basin currents, involved in their formation (ATC and BATC), are most intense and energetic in this season (Figure 17a).

The ABV, the MRV and the ISV are located along the southern and the eastern coast of Sicily where the wind stress curl is steadily cyclonic (Figures 2d, 4c, 4d). Their strength and their interannual variability are influenced by the temporal evolution of the wind stress amplitude and vorticity (Figures 15, 17b).

The SMG is located on the margins of the African shelf break (Figures 1a, 2a, 2b) and its vertical extension affects the entire water column (maximum depth of 400 m) as documented by the float WMO 1900629 (Figure 13); the wind stress is weak and dimly cyclonic in this region (Figure 2 lower panels). Therefore, we define the SMG in Figure 17b as strongly influenced by the interaction between the surface currents and the topography.

The mesoscale structures located in regions where the influence of the wind stress is lower can be forced by the large-scale internal variability of the ocean. An example of this interaction is the SISV, whose interannual variability is connected to the decadal variability of the surface circulation in the northern Ionian (Figure 15a). However, the most representative example of the influence of internal forcing on the variability of a mesoscale structure is the NSA. This anticyclone, although located in the southern Tyrrhenian Sea, is affected by the decadal variability induced by the adjacent Ionian Sea (Figure 6). This result, as suggested by [27], opens to a new interpretation of the link between different Mediterranean sub-basins and underlines the importance of internal processes on the variability of the mesoscale structures.

In summary, the surface circulation in the SC and southern Tyrrhenian Sea is characterized by multi-scale spatial and temporal variability. The main spatial scales involved are the basin, sub-basin and mesoscale. The main temporal scales involved are the seasonal, interannual and

decadal scales. In this work, the complexity of the SC current system was investigated by combining different in-situ data and satellite products. Results provide an updated picture of the surface circulation, detecting new mesoscale features and describing their temporal variability and strength in relation to the main external and/or internal forcings. The winter strengthening of the wind stress directly influence most of the structure stronger in this season. The structures stronger in summer and/or located in high dynamical regions are mainly driven by the instability of the surface current and/or by their interaction with the bottom topography. In the regions where the influence of the external forcings is weaken, the large-scale internal variability of the adjacent Mediterranean basins can influence the local dynamics.

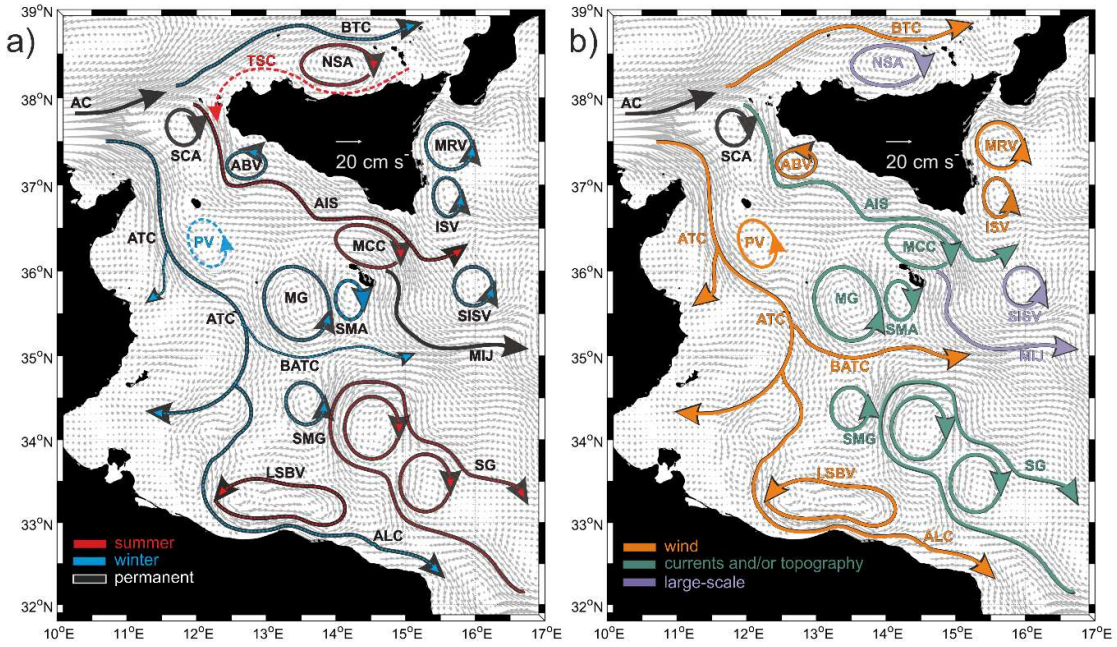

Figure 17. Schematized representation of the mean surface circulation in the Sicily Channel and Southern Tyrrhenian Sea (black arrows) based on the mean optimal currents circulation map depicted Figure 2b (bright grey vectors). (a) Black arrows emphasized the permanent sub-basin and mesoscale structures; dashed red/blue lines emphasized the seasonal summer/winter structures, respectively; red/blue arrows are superimposed on the black arrows when the structures are permanent but most intense in summer/winter respectively. (b) Sub-basin and mesoscale structures are classified according to the mechanisms that drive them: the wind forcing (orange arrows), the interaction between currents and topographical forcings (light green arrows), the large-scale internal processes (light purple arrows).

Author Contributions: writing—original draft preparation, M.M.; writing—review and editing, P.-M.P., D.C., A.Doglioli, G.N. and R.G.; investigation, M.M. and P.-M.P.; data curation, M.M., G.N., R.G., D.C. and M.-H.R.; formal analysis, M.M., G.N. and R.G.; resources, D.C., M.-H.R., A.G. and R.S.; funding acquisition, P.-M.P. and A.Drago.

Funding: This research was mainly funded by the Italian Ministry of Education, University and Research as part of the Argo-Italy program, and partly funded by the Italia-Malta Programme – Cohesion Policy 2007–2013, European Union Regional Development Funds (ERDF) through the CALYPSO and CALYPSO FO projects,. The program MISTRALS of CNRS funded the drifters deployed during the PEACETIME cruise (Guieu C., Desboeufs K., 2017, RV Pourquoi pas ?, https://doi.org/10.17600/17000300).

Acknowledgments: The authors would like to thanks all the people who have deployed drifters and made their data available in the Mediterranean Sea in the period 1993-2018. We acknowledge Antonio Bussani for his

technical support and his work in the production of the Mediterranean drifter dataset, and Elena Mauri for her constructive comments. We thank the two anonymous reviewers for their constructive comments on the manuscript.

Conflicts of Interest: The authors declare no conflict of interest.

References

1. Sorgente R.; Olita, A.; Oddo, P.; Fazioli, L.; Ribotti, A. Numerical simulation and decomposition of kinetic energy in the Central Mediterranean: insight on mesoscale circulation and energy conversion. Ocean Sci. **2011**, 7, 503-519. doi:10.5194/os-7-503-2011.
2. Schroeder, K.; Chiggiato, J.; Josey, S.A.; Borghini, M.; Aracri, S.; Sparnocchia, S. Rapid response to climate change in marginal sea. Sci. Rep. **2017**, 7:4065, doi:10.1038/s41598-017-04455-5.
3. Jouini, M.; Béranger, K.; Arsouze, T. J.; Beuvier, S.; Thiria, M.; Crepon, I. Taupier-Letage, I. The Sicily Channel surface circulation revisited using a neural clustering analysis of a high-resolution simulation, J. Geophys.Res. Oceans **2016**, 121, 4545–4567, doi: https://doi.org/10.1002/2015JC011472.
4. Ferron, B.; Bouruet Aubertot, P.; Cuypers, Y.; Schroeder, K.; Borghini, M. How important are diapycnal mixing and geothermal heating for the deep circulation of the Western Mediterranean? Geophys. Res. Lett. **2017**, 44, 15, 7845-7854, doi: https://doi.org/10.1002/2017GL074169.
5. Vladoui, A.; Bouruet-Aubertot P.; Cuypers, Y.; Ferron, B.; Schroeder, K.; Borghini, M.; Leizour, S.; Ben Ismail, S. Turbulence in the Sicily Channel from microstructure measurements. Deep-Sea Res. I **2018**, 137, 97-122, doi: https://doi.org/10.1016/j.dsr.2018.05.006.
6. Millot, C.; Taupier-Letage, I. Circulation in the Mediterranean Sea. Handb. Environ. Chem. **2005**, 5(K), 29-66.
7. Lermusiaux, P.F.J.; Robinson, A.R. Features of dominant mesoscale variability, circulation patterns and dynamics in the Strait of Sicily. Deep-Sea Res. I **2001**, 48, 1953-1997.
8. Béranger, K.; L. Mortier; Gasparini, G.-P.; Gervasio, L.; Astraldi, M.; Crepon, M. The dynamics of the Sicily Strait: A comprehensive study from observations and models, Deep Sea Res. II, 2004, 51, 411–440.
9. Poulain, P. M.; Zambianchi, E. Surface circulation in the central Mediterranean Sea as deduced from Lagrangian drifters in the 1990s. Cont. Shelf Res. **2007**, 27, 981–1001.
10. Astraldi, M.; Balopoulos, S.; Candela, J.; Font, J.; Gacic, M.; Gasparini, G. P.; Manca, B.; Theocharis, A.; Tintoré, J. The role of straits and channels in understanding the characteristics of Mediterranean circulation, Prog. Oceanogr. **1999**, 44, 65–108.
11. Poulain, P.-M.; Menna, M.; Mauri, E. Surface geostrophic circulation of the Mediterranean Sea derived from drifter and satellite altimeter data. J. Phys. Oceanogr. **2012**, 42(6), 973–990. https://doi.org/10.1175/JPO-D-11-0159.1.
12. Pinardi, N.; Zavatarelli, M.; Adani, M.; Coppini, G.; Fratianni, C.; Oddo, P.; Simoncelli, S.; Tonani, M.; Lyubartsev, V.; Dobricic, S.; Bonaduce, A. Mediterranean Sea large-scale low-frequency ocean variability and water mass formation rates from 1987 to 2007: a retrospective analysis (ISSN 0079-6611). Prog. Oceanogr. **2015**, 132, 318–332. https://doi.org/10.1016/j.pocean.2013.11.003.
13. Molcard, A.; Gervasio, L.; Griffa, A.; Gasparini, G. P.; Mortier, L.; Ozgokmen, T. M. Numerical investigation of the Sicily Channel dynamics: density currents and water mass advection, J. Mar. Syst. **2002**, 36, 219–238.
14. Amores A.; Jordà, G.; Arsouze, T.; Le Sommer, J. Up to what extent can we characterize ocean eddies using present day gridded altimetric products? J. Geophys. Res.-Oceans **2018**, 123, https://doi.org/10.1029/2018JC014140.
15. Ciani, D.; Rio, M.-H.; Menna, M.; Santoleri R. A synergetic approach for the space-based sea surface currents retrieval in the Mediterranean Sea, Remote Sens. **2019**, 11, 1285, doi:10.3390/rs11111285.
16. Menna, M.; Gerin, R.; Bussani, A.; Poulain, P.-M. The OGS Mediterranean drifter database: 1986-2016. Technical report 2017/92 Sez. OCE 28 MAOS, 2017.
17. Menna, M.; Poulain, P.-M.; Bussani, A.; Gerin, R. Detecting the drogue presence of SVP drifters from wind slippage in the Mediterranean Sea, Measurement **2018**, 125, 447-453, https://doi.org/10.1016/j.measurement.2018.05.022.

18. Rio, M.H.; Pascual, A.; Poulain, P.-M.; Menna, M.; Barcelò, B.; Tintorè, J. Computation of a new mean dynamic topography for the Mediterranean Sea from model outputs, altimeter measurements and oceanographic in situ data, Ocean Sci. **2014**, 10, 731–744, doi: http://dx.doi.org/10.5194/os-10-731-2014.
19. Poulain P.-M.; Barbanti R.; Font J.; Cruzado A.; Millot C.; Gertman I.; Griffa A.; Molcard A.; Rupolo V.; Le Bras S.; Petit de la Villeon L. MedArgo: a drifting profiler program in the Mediterranean Sea. Ocean Sci **2007**, 3:379–395.
20. Rio, M.H.; Santoleri, R. Improved global surface currents from the merging of altimetry and Sea Surface Temperature data. Remote Sens. Environ. **2018**, 216, 770–785. https://doi.org/10.1016/j.rse.2018.06.003.
21. Piterbarg, L.I. A simple method for computing velocities from tracer observations and a model output. Appl. Mat. Model. **2009**, 33, 3693–3704. https://doi.org/10.1016/j.apm.2008.12.006.
22. Atlas, R.; Hoffman, R.N.; Ardizzone, J.; Leidner, S.M.; Jusem, J.C.; Smith, D.K.; Gombos, D. A cross-calibrated, multiplatform ocean surface wind velocity product for meteorological and oceanographic applications. B. Am. Meteorol. Soc. **2011**, 92, 157-174, doi: 10.1175/2010BAMS2946.1.
23. Shabrang, L.; Menna, M.; Pizzi, C.; Lavigne, H.; Civitarese, G.; Gačić, M. Long-term variability of the southern Adriatic circulation in relation to North Atlantic Oscillation. Ocean Sci. **2016**, 12 (1), 233-241, doi: https://doi.org/10.5194/os-12-233-2016.
24. Menna, M.; Reyes Suarez, N.C.; Civitarese, G.; Gacic, M.; Poulain, P.-M.; Rubino, A. Decadal variations of circulation in the Central Mediterranean and its interactions with the mesoscale gyres. Deep Sea Res.-Oceans II **2019**, in press, https://doi.org/10.1016/j.dsr2.2019.02.004.
25. Aulicino, G.; Cotroneo, Y.; Lacava, T.; Sileo, G.; Fusco, G.; Carlon, R.; Satriano, V.; Tramutoli, V.; Budillon, G. Results of the first wave glider experiment in the southern Tyrrhenian Sea. Adv. Oceanogr. Limnol. **2016**, 7(1), 16-35, doi: 10.4081/aiol.2016.5682.
26. Ciappa, A.C. Surface circulation patterns in the Sicily Channel and Ionian Sea as revealed by MODIS chlorophyll images from 2003 to 2007. Contin. Shelf Res. **2009**, 29, 2099-2109, doi:10.1016/j.csr.2009.08.002.
27. Rubino, A.; Zanchettin, D.; Androsov, A.; Voltzinger, N-E. Tidal record as liquid climate archives for large-scale interior Mediterranean variability. Sci. Rep. **2018**, 8:12586, doi:10.1038/s41598-018-30930-8.
28. Drago, A.; Ciraolo, G.; Capodici, F.; Cosoli, S.; Gacic, M.; Poulain, P.-M.; Tarasova, R.; Azzopardi, J.; Gauci, A.; Maltese, A.; Nasello, C.; La Loggia, G. 'CALYPSO – An operational network of HF radars for the Malta-Sicily Channel', Proceedings of the Seventh International Conference on EuroGOOS 28–30 October 2014, Lisbon, Portugal, Edited by H. Dahlin, N.C. Fleming and S. E. Petersson. First Published 2015. Eurogoos Publication no. 30. ISBN 978-91-974828-9-9.
29. Capodici, F.; Cosoli, S.; Ciracolo, G.; Nasello, C.; Maltese, A.; Poulain, P.-M.; Drago, A.; Azzopardi, J.; Gauci, A. Validation of HF radar sea surface currents in the Malta-Sicily Channel. Remote Sens. Environ **2019**, 225, 65-76. https://doi.org/10.1016/j.rse.2019.02.026.
30. Pinardi, N.; Navarra, A. Baroclinic wind adjustment processes in the Mediterranean Sea, Deep-Sea Res. II **1993**, 40, 1299–1326.